# Electronic Structure Calculations on Active Site Models for 4-Fe, 4-S Iron–Sulfur Proteins

**Arie Aizman and David A. Case***

*Contribution from the Department of Chemistry, University of California, Davis, California 95616.* *Received September 17, 1981*

**Abstract:** Molecular orbital calculations in the Xα multiple-scattering approximation are reported for $[Fe_4S_4(SH)_4]^{2-}$ and $[Fe_4S_4(SCH_3)_4]^{2-}$, models for the active site in certain ferredoxins and "high-potential" iron–sulfur proteins. Both $T_d$ and $D_{2d}$ nuclear geometries are considered; in addition, "broken symmetry" unrestricted calculations are reported in which the orbitals have only $C_{2v}$ symmetry. The energy ordering of iron d levels is different from any predicted on the basis of qualitative molecular orbital theory or from earlier Xα calculations that assumed a cube geometry. The unrestricted calculations show that these clusters may be thought of as arising from the antiferromagnetic coupling of two reduced 2Fe–2S clusters and predict a Heisenberg exchange constant of $-190$ cm$^{-1}$. This model is in qualitative agreement with magnetic susceptibility, NMR, and Mössbauer results. Features in the optical spectrum are qualitatively assigned to d–d and charge-transfer transitions. Contour plots show the nature of the orbitals involved in oxidation and reduction processes.

The structures and properties of iron–sulfur electron-transport proteins have been the subject of extensive investigations, as the number of biological reactions known to involve such clusters continues to grow. Clusters involving one, two, three, and four iron atoms have been identified and have been implicated in electron transport, enzymatic activity, energy transduction, and regulation. Proceeding apace have been synthetic efforts to make model complexes whose structural, spectroscopic, and oxidation–reduction properties mimic those found in natural systems. Several comprehensive reviews are available that detail the remarkable progress that has been made.[1-5]

Proteins containing 4Fe–4S clusters have been found to exist in three oxidation states, corresponding to the formal overall oxidation numbers $(Fe_4S_4)^{1+,2+,3+}$. The midpoint reduction potentials for both the 1+/2+ and the 2+/3+ couples vary by about 700 mV in known proteins. This variability apparently allows these proteins to participate in a wide variety of electron-transport chains. Several qualitative attempts have been made to describe their electronic structures and spin distributions, but until recently weakly interacting multinuclear transition-metal clusters such as these have been outside the scope of computational quantum chemistry. Advances in computers and improvements in codes have now made Xα multiple-scattering calculations feasible for these systems. As part of a continuing project to describe the electronic properties of one-, two-, and four-iron clusters at a common level of approximation,[6-8] we present here Xα calculations on $[Fe_4S^*_4(SH)_4]^{2-}$ and $[Fe_4S^*_4(SCH_3)_4]^{2-}$ as models for the active site of oxidized four-iron ferredoxin and reduced "high-potential" iron–sulfur proteins.

As with other complicated systems, it is useful to discuss the electronic structures of these complexes in terms of idealized limiting models. Perhaps the simplest of these is *closed-shell molecular orbital theory*, which has been applied to these clusters both in a qualitative fashion[9,10] and through approximate calculations, invoking the Slater exchange potential.[8,11] This model yields a singlet wavefunction in which all of the iron atoms are equivalent and the d electrons are extensively delocalized. As we discuss below, such a model can be useful for obtaining a qualitative understanding of the nature of the optical spectra, but it has serious deficiencies in its description of the ground and low-lying excited states. The problems arise for much the same reason that the theory fails for $H_2$ at large internuclear distances: when the overlap of atomic orbitals on two or more centers becomes very small, an MO description assigning electrons of both spins to each center is inappropriate. In this case the iron d–d interactions are quite weak, and the closed-shell solution is unstable to perturbations that allow electron spins to localize at the iron centers. We show below that in the closed-shell MO model this lack of correlation between electrons of opposite spin leads to observable effects, most notably a failure to predict the existence of low-lying paramagnetic excited states.

At the opposite extreme is an idealized *valence bond picture* in which each iron atom has five or six d electrons that couple among themselves to form high-spin states with $S = {}^5/_2$ or 2; these spins then interact with their neighbors via antiferromagnetic exchange interactions. For the $(Fe_4S_4)^{2+}$ oxidation state considered here, there are formally two Fe(II) and two Fe(III) ions. A model qualitatively consistent with experimental data is depicted in Figure 1. Antiferromagnetic coupling between the iron atoms is imagined to occur via 90° superexchange through the sulfur atoms. There is delocalization of the sixth 3d electron between the two spin-α iron atoms and between the two spin-β iron atoms. Effectively, each iron atom is $Fe^{2.5+}$ and has the same charge distribution, but there are two sets of irons with inequivalent spin distributions. We discuss below the experimental evidence leading to such a model,[12] but it is clear that it can only be an idealization, since any covalent effects with the sulfur ligands are ignored.

What is required for actual computations is a method that can interpolate between the MO and VB limits outlined above. A generalized valence bond (GVB) calculation could do this, although difficulties would be encountered since the perfect-pairing approximation does not hold here. To our knowledge, no GVB calculations containing more than two spin-coupled transition-metal atoms have been reported. We have chosen instead a somewhat simpler method, an unrestricted Hartree–Fock (UHF) wavefunction, in which both space and spin restrictions are relaxed. This approach retains the computational advantages of a self-

(1) "Iron-Sulfur Proteins", Lovenberg, W., Ed.; Academic Press: New York, 1973; Vol. I and II; 1977, Vol. III.
(2) Averill, B. A.; Orme-Johnson, W. H. In "Metal Ions in Biological Systems"; Sigel, H., Ed.; Marcel Dekker: New York, 1978; Vol. VII.
(3) Sweeney, W. V.; Rabinovitz, J. C. *Annu. Rev. Biochem.* **1980**, *49*, 139.
(4) Holm, R. H.; Ibers, J. A. *Science (Washington, D.C.)* **1980**, *209*, 223.
(5) See, especially: Holm, R. H.; Ibers, J. A., in Ref. 1, Vol. III, pp 206–281. Cammack, R.; Dickson, D. P. E.; Johnson, C. E., in Ref. 1, Vol. III, pp 283–330.
(6) 1-Fe models: Norman, J. G., Jr.; Jackels, S. C. *J. Am. Chem. Soc.* **1975**, *97*, 3833.
(7) 2-Fe models: Norman, J. G., Jr.; Kalbacher, B. J.; Jackels, S. C. *J. Chem. Soc., Chem. Commun.* **1978**, 1027. Norman, J. G., Jr.; Ryan, P. B.; Noodleman, L. *J. Am. Chem. Soc.* **1980**, *102*, 4279.
(8) 4-Fe models: Yang, C. Y.; Johnson, K. H.; Holm, R. H.; Norman, J. G., Jr. *J. Am. Chem. Soc.* **1975**, *97*, 6596.
(9) Thomson, A. J. *Biochem. Soc. Trans.* **1975**, *3*, 468. *J. Chem. Soc., Dalton Trans.* **1981**, 1180.
(10) Geurts, P. J. M.; Gosselink, J. W.; van der Avoird, A.; Baerends, E. J.; Snijders, J. G. *Chem. Phys.* **1980**, *46*, 133.
(11) Averill, B. A.; Herskovitz, T.; Holm, R. H.; Ibers, J. A. *J. Am. Chem. Soc.* **1973**, *95*, 3523.
(12) Dickson, D. P. E.; Johnson, C. E.; Thompson, C. L.; Cammack, R.; Evans, M. C. W.; Hall, D. O.; Rao, K. K.; Weser, U. *J. Phys. (Orsay, Fr.)* **1974**, *35*, C6-343.

0002-7863/82/1504-3269$01.25/0 

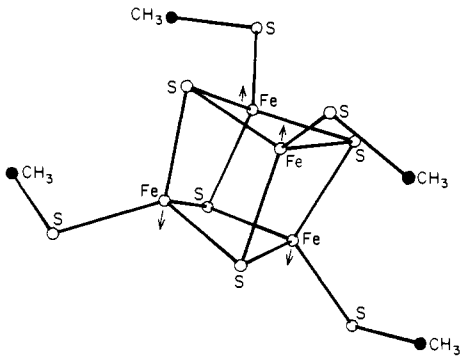


**Figure 1.** Illustration of a 4-Fe, 4-S cluster model in the $D_{2d}$ geometry (geometry **4** of Table I). Arrows show the spin orientation of the iron d orbitals in the idealized VB model (see text).

consistent field molecular orbital scheme while allowing a proper qualitative description of weakly coupled spin systems. A principal disadvantage of the UHF model is that the wavefunctions are not spin eigenfunctions. This can be ameliorated to some extent by spin-projection techniques; further, the qualitative features of the orbitals are similar to those of the GVB scheme. The results reported here are thus the first that derive from wave functions that are qualitatively correct for clusters of this sort.

The general nature of instabilities in the restricted Hartree–Fock procedure is the subject of much current investigation,[13] but it is well established that the type encountered here should be expected whenever the energy difference between occupied and unoccupied molecular orbitals becomes small.[14,15] This will be the case when orbital overlaps are small, and a lower energy solution should be expected in which the $\alpha$ spins are concentrated on one center, with the $\beta$ spins at the other center. A careful analysis of the unrestricted approach to the $H_2$ problem has been presented by Fukotome.[16] Early computational applications of space-unrestricted Hartree–Fock theory concentrated on core ionizations,[17] but more recently a variety of applications to multinuclear transition-metal clusters have appeared.[18,19] X$\alpha$ multiple-scattering calculations have been reported for metal–metal bonded systems[19] and for 2-Fe iron–sulfur clusters.[7] Noodleman and Norman have called these "X$\alpha$ valence bond" calculations to emphasize their ability to handle weak coupling situations, even though they do not rely on structures built from atomic orbitals, as in the original valence bond method. In conjunction with spin-projection techniques, this approach can yield estimates for antiferromagnetic exchange coupling constants; this makes unrestricted X$\alpha$ calculations a powerful extension of the conventional MO theories of multinuclear transition-metal systems.

A previous X$\alpha$ multiple-scattering calculation on a 4Fe–4S cluster has been reported by Yang, Johnson, Holm, and Norman.[8] Our present results extend this work in several directions, using a more realistic geometry than before, incorporating overlapping spheres, and adopting an unrestricted model for the spin distributions. Comparisons of the new and old results are given below. We are grateful to these authors for providing us with the details of their calculations, which were used as a starting point for those reported here.

The details of our calculations and the geometries we have chosen are discussed in the next section. Following that, we present results for the closed-shell molecular orbital model and compare our results to previous calculations. These are used to discuss optical spectra and the possibility of a Jahn–Teller instability in idealized $T_d$ geometries. The next section gives results for the unrestricted calculations and considers magnetic susceptibility, NMR, and Mössbauer experimental data. We estimate an antiferromagnetic coupling constant and discuss the implications of our results for the oxidation–reduction behavior of the proteins.

Table I. Geometries Used in the Calculations

| | geometry[a] | | |
|---|---|---|---|
| | 1 | 2 | 3, 4[b] |
| | (a) Cartesian Coordinates[c] | | |
| Fe | −2.145 | −1.835 | −1.854 |
| | 2.145 | 1.835 | 1.854 |
| | 2.145 | 1.835 | 1.797 |
| S | −4.601 | −4.291 | −4.297 |
| | 4.601 | 4.291 | 4.297 |
| | 4.601 | 4.291 | 4.278 |
| S* | −2.145 | −2.412 | −2.436 |
| | 2.145 | 2.412 | 2.436 |
| | −2.145 | −2.412 | −2.356 |
| H | −6.071 | −5.754 | −3.607 |
| | 6.071 | 5.754 | 3.607 |
| | 6.071 | 5.754 | 6.616 |
| | (b) Bond Lengths and Angles[d] | | |
| Fe-Fe | 3.211 | 2.746 | 2.732 (4), 2.776 (2) |
| Fe-S* | 2.270 | 2.286 | 2.239 (4), 2.310 (8) |
| S*-S* | 3.211 | 3.61 | 3.586 (4), 3.645 (2) |
| Fe-Fe-Fe | 90 | 60.0 | 59.5 (8), 61.1 (4) |
| Fe-S*-Fe | 90 | 73.8 | 73.8 |
| S*-Fe-S* | 90 | 104.1 | 104.1 |
| Fe-S-H | 180 | 180.0 | 103.0 |

[a] The numbering scheme, 1–4, is described in the text. [b] In 4, H is replaced with a methyl group whose unique atom coordinates are C(−3.352,3.352, 7.472), H(−4.441,4.441,8.870), and H(−1.321,3.725,7.733). The Fe-S-C angle is 103.0° and the S-C bond length is 1.832 Å. [c] The $x$, $y$, and $z$ coordinates are given for each unique atom, in atomic units. [d] In Å and deg.

## Details of the Calculations

The X$\alpha$ multiple-scattering method has been the subject of several recent reviews,[20–22] and the compact clusters considered here appear to be well-suited to the approximations involved. Recent improvements[23] in computer codes proved quite important for these high-symmetry cases, cutting computing time by more than a factor of 4. Here we give the details specific to these calculations and discuss the geometries chosen to model the active sites of the proteins.

**Geometries.** We have considered four geometries in this work, three for $[Fe_4S_4^*(SH)_4]^{2-}$ and one for $[Fe_4S_4^*(SCH_3)_4]^{2-}$. These are labeled **1**–**4** in Table I. The first (**1**) was that used earlier by Yang et al.[8] This was considered for comparison purposes only, since it is unrealistic in assuming the iron and sulfur atoms to be at the corner of a cube. This leads to equal Fe–Fe and S*–S* bond lengths, whereas the averages in model compounds[11,27] are 2.75 and 3.61 Å, respectively; similar values are found in proteins.[28] The cube model also imposes 90° S*–Fe–S* and Fe–S*–Fe angles, while observed values are 104.1° and 73.8°. This cube geometry

(13) Benard, M.; Paldus, J. *J. Chem. Phys.* **1980**, *72*, 6546 and references therein.
(14) Lowdin, P. O. *Rev. Mod. Phys.* **1962**, *34*, 80; **1964**, *36*, 968.
(15) Ginsberg, A. P. *Inorg. Chim. Acta, Rev.* **1971**, *5*, 45.
(16) Fukotome, H. *Prog. Theor. Phys.* **1972**, *47*, 1156.
(17) Bagus, P. S.; Schaefer, H. F. *J. Chem. Phys.* **1972**, *56*, 224.
(18) Benard, M. *J. Chem. Phys.* **1979**, *71*, 2546.
(19) Noodleman, L.; Norman, J. G., Jr. *J. Chem. Phys.* **1979**, *70*, 4903. Noodleman, L. *Ibid.* **1981**, *74*, 5737.
(20) Connolly, J. W. D. In "Modern Theoretical Chemistry"; Segal, G. A., Ed.; Plenum Press: New York, 1976; Vol. IV.
(21) Johnson, K. H. *Annu. Rev. Phys. Chem.* **1975**, *26*, 39.
(22) Case, D. A. *Annu. Rev. Phys. Chem.* **1982**, to be published.
(23) Case, D. A.; Yang, C. Y. *Int. J. Quantum Chem.* **1980**, *18*, 1091. Other general improvements in efficiency were coded by D. A. Case, M. Cook, and S. F. Sontum.
(24) Rösch, N.; Klemperer, W. G.; Johnson, K. H. *Chem. Phys. Lett.* **1973**, *23*, 149.
(25) Case, D. A.; Cook, M.; Karplus, M. *J. Chem. Phys.* **1980**, *73*, 3294.
(26) Norman, J. G., Jr. *Mol. Phys.* **1976**, *31*, 1191.
(27) (a) Berg, J. M.; Hodgson, K. O.; Holm, R. H. *J. Am. Chem. Soc.* **1979**, *101*, 4586. (b) Laskowski, E. J.; Frankel, R. B.; Gillum, W. O.; Papaefthymiou, G. C.; Renaud, J.; Ibers, J. A.; Holm, R. H. *J. Am. Chem. Soc.* **1978**, *100*, 5322. (c) Holm, R. H.; Phillips, W. D.; Averill, B. A.; Mayerle, J. J.; Herskovitz, T. *J. Am. Chem. Soc.* **1974**, *96*, 2109.
(28) Adman, E. T.; Sieker, L. C.; Jensen, L. H. *J. Biol. Chem.* **1976**, *25*, 3801. Carter, C. W., Jr.; Kraut, J.; Freer, S. T.; Alden, R. A. *Ibid.* **1974**, *248*, 6339.

was originally chosen to investigate analogies between iron–sulfur complexes and metallic iron but is not really adequate for a detailed description of the former. A much improved idealized geometry, (**2**), still with $T_d$ symmetry, can be constructed by allowing the iron and sulfur tetrahedra to have different sizes. In this way the bond lengths and angles mentioned above achieve the average values seen experimentally. Exterior to the $Fe_4S_4$* core, such a model mimics the cysteinyl group with linear SH ligands. This is undoubtedly a major shortcoming, but is required if one is to maintain $T_d$ symmetry. As we discuss below, this model has many features in common with our more elaborate calculations but is quite different from the results found earlier for the cube geometry.

There are two major reasons for extending the calculations to $D_{2d}$ nuclear geometries. First, this allows the external Fe–S–R angle to be reduced from 180° to values near the 103° seen in model complexes. The hydrogen atom may also be replaced with a methyl group at this point. Second, a distortion of the core to provide unequal Fe–Fe, Fe–S*, and S*–S* bond lengths is possible in the lower symmetry. The distortion seen in the model $[Fe_4S_4*(SCH_2Ph)_4]^{2-}$ has four "short" Fe–S* lengths averaging 2.24 Å and eight "long" ones averaging 2.31 Å.[11] We have used this structure as a guide for our $D_{2d}$ calculations of $[Fe_4S_4*(SH)_4]^{2-}$ (**3**) and $[Fe_4S_4*(SCH_3)_4]^{2-}$ (**4**). Geometries and internal coordinates for both the $T_d$ and $D_{2d}$ structures are collected in Table I. Other types of $D_{2d}$-like distortions are seen in complexes with one more or one less electron;[27] such structures will be discussed in future publications.

**Method.** Many features of the computational method are similar to previous work.[6,7,25,29] $\alpha$ factors for the exchange potential were those determined by Schwarz from atomic calculations.[30] Partial waves through $l = 4$ were used on the outer sphere, through $l = 2$ on Fe, through $l = 1$ on C and S, and through $l = 0$ on H. This corresponds to a minimal angular basis, but it should be remembered that the radial portion of these orbitals is determined numerically and is different for each molecular orbital. A "Watson" sphere with charge 2+ and a radius equal to the outer-sphere radius was used to mimic the electrostatic potential of the cations.

Two procedures are often used to calculate charge and spin distributions. The integrated charges inside the atomic spheres are obtained directly from the multiple-scattering solution but do not sum to unity for each orbital since some charge is in the intersphere and outer-sphere regions. An alternative procedure is to partition the intersphere and outer-sphere charge among the atoms according to the algorithm of Case and Karplus.[25] This produces values that may be more easily compared to Mullikan populations derived from basis-set calculations. It has the disadvantage that the partitioning scheme is arbitrary. Except where noted, all charge and spin distributions given below use the partitioned values.

One important feature of multiple-scattering calculations is the choice of sphere radii for the cells surrounding each atom. In recent years much use has been made of overlapping cells, which has been shown to lead to improved energy spacings, particularly for "open" molecules.[24,25] For relatively compact molecules, the choice of cell radii is expected to be less crucial. We have studied this with calculations on $[Fe_4S_4(SH)_4]^{2-}$, using the geometry previously considered by Yang et al.[8] As a check of our computer codes, we reproduced these earlier results, which use nonoverlapping cells, and have compared these results to a second calculation incorporating sphere overlap. Following a suggestion of Norman,[26] this second calculation used values equal to 85% of the atomic number radii obtained from a superposition of atomic charge densities. (The superposition was done for geometry **2**, the most realistic $T_d$ structure.) The factor of 85% was chosen to satisfy approximately the virial theorem, yielding a ratio of $-2\langle T\rangle/\langle V\rangle$ of 1.0008, compared to 1.57 for the touching spheres. The sphere radii for both calculations are given in Table II.

Table II. Sphere Radii[a]

| | Yang et al.[b] | present |
|---|---|---|
| Fe | 2.286 | 2.312 |
| S | 1.974 | 2.411 |
| S* | 2.003 | 2.394 |
| C | 1.486 | 1.678 |
| H | 0.573[c] | 1.293 |

[a] Values in atomic units. [b] Reference 8. [c] For $[Fe_4S_4(SH)_4]^{2-}$; a value of 0.626 was used for $[Fe_4S_4(SCH_3)_4]^{2-}$.

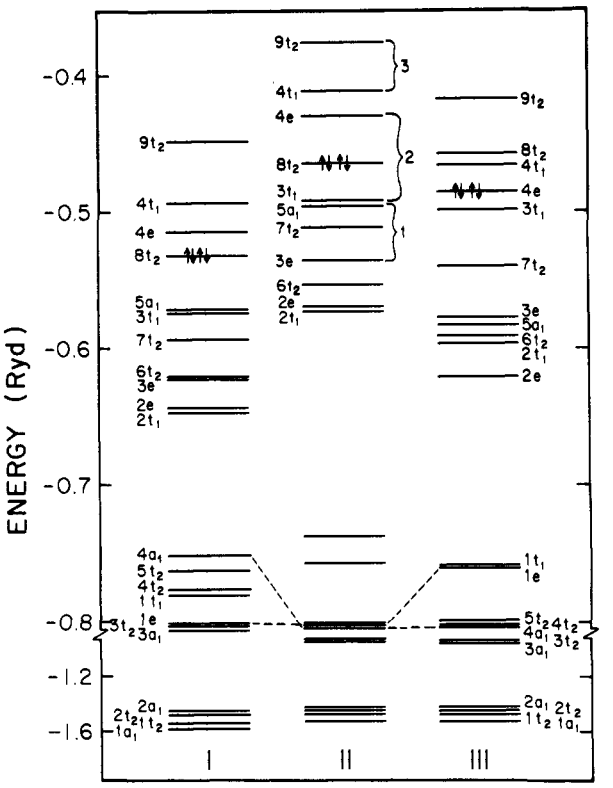


**Figure 2.** Molecular orbital energies for $[Fe_4S_4(SH)_4]^{2-}$: column I gives results from ref 8, using geometry **1**; column II is the same as column I, but using overlapping spheres; column III uses geometry **2** with overlapping spheres. Labels 1, 2, and 3 in the center column identify the bonding, nonbonding, and antibonding orbitals of the simple MO scheme, as discussed in the text. Arrows give the electron occupation in the highest occupied orbital.

(Outer-sphere sizes were chosen in all cases to be tangent to the atomic spheres.) In addition to an increase in the average size of the atomic spheres when overlap is incorporated, there are important changes in the relative sizes. In particular, in the older calculation the iron spheres were larger than the sulfur spheres, while the reverse is true in the present work. The latter order seems more consistent with observed Fe–Fe and S*–S* bond lengths of 2.75 and 3.61 Å, respectively. The new hydrogen spheres are also much larger than their nonoverlapping counterparts; these newer cells contain 0.76 electron each, while the total charge inside each H sphere in the old calculation was only 0.07 electron. The larger value is expected to yield a more realistic wavefunction, at least as measured by one-electron properties.[25]

Valence electron energies are shown in the first two columns of Figure 2. The ordering of levels is nearly identical in the two calculations, the main difference being the somewhat wider spacing of the valence levels in the second calculation. In the upper valence region, two pairs of orbitals reverse their order: $5a_1/3t_1$ and $3e/6t_2$. In the lower valence region, the $4a_1$ orbital (75% S* 3p character) drops considerably in energy, from the top to the bottom of the "band" of predominant S* 3p character. The top occupied and the lowest unoccupied orbitals are the same in the two calculations, with a slightly larger HOMO–LUMO gap in the results that incorporate sphere overlap. For the purposes for which we intend to use the wave functions, these differences are minor. However,

(29) Case, D. A.; Karplus, M. *J. Am. Chem. Soc.* **1977**, *99*, 6182.
(30) Schwarz, K. *Phys. Rev. B: Solid State* **1972**, *5*, 2466.

since we do expect the energies from the calculation with overlap to be somewhat more realistic,[24-26] we continue this procedure in subsequent calculations. The virial ratios for all the calculations reported here range from 1.0006 to 1.0009.

With these parameters we performed conventional spin-restricted MO calculations for $[Fe_4S_4(SH)_4]^{2-}$ in geometries **2** and **3** and for $[Fe_4S_4(SCH_3)_4]^{2-}$ in geometry **4**. We also performed a spin-unrestricted, space-restricted calculation in geometry **4** on a high-spin state with $M_s = 9$ (i.e., with 18 more electrons of spin $\alpha$ than of spin $\beta$). This should be close to a spin eigenfunction with $S = 9$, corresponding to a valence bond picture in which all of the iron atoms have their spins in the same direction (a ferromagnetic rather than an antiferromagnetic state). Details of the occupation scheme for this calculation will be given below. Computer times per SCF iteration were 5, 14, and 43 s for the $T_d$ spin-restricted, $D_{2d}$ spin-restricted, and $D_{2d}$ spin-unrestricted calculations, respectively, on the CDC 7600 machine at Lawrence Berkeley Laboratory. (The last number is for $[Fe_4S_4(SCH_3)_4]^{2-}$, while the first two are for $[Fe_4S_4(SH)_4]^{2-}$.) Twenty to forty iterations were required to a relative convergence of $5 \times 10^{-4}$ in the potential; this is equivalent of an accuracy of $1 \times 10^{-5}$ hartree in the valence one-electron energies.

The spin- and space-unrestricted calculation proved to be more difficult to converge. This wave function has $M_s = 0$ and uses geometry **4** but assumes that the orbitals have only $C_{2v}$ symmetry. This removes the symmetry equivalence of the "top" and "bottom" of the molecule (Figure 1). We began with a restricted potential from the $D_{2d}$ calculation on $[Fe_4S_4(SCH_3)_4]^{2-}$. Upon descent from $D_{2d}$ to $C_{2v}$ symmetry (removing the $S_4$ symmetry operator) the degenerate E representation splits into $B_1 + B_2$. The sum of the two E orbitals must have equivalent occupation on all four iron atoms, but this need not be the case for $B_1$ or $B_2$ separately, even if the potential has $D_{2d}$ symmetry. We took advantage of this feature by dividing the $B_1$ and $B_2$ orbitals into a first set with more density at the top of the molecule and a second set with more density at the bottom. Those in the first set were assigned spin $\alpha$, while those at the bottom were assigned spin $\beta$. (At this point, the top and bottom orbitals occurred in degenerate pairs, since the potential was still a restricted $D_{2d}$ potential.) These new occupations produced a slight excess (0.7 electron) of $\alpha$ spin over $\beta$ spin at each iron atom at the top of the molecule (and an equal excess of $\beta$ spin over $\alpha$ at the bottom). Upon iterating in spin-unrestricted $C_{2v}$ symmetry, the excess of $\alpha$ spin at the top continued to grow until it reached a converged value of 2.92. At each iteration, orbitals of all four symmetries ($A_1$, $A_2$, $B_1$, $B_2$) appear in degenerate pairs, with every spin-$\alpha$ orbital being matched with its $S_4$ image having spin $\beta$. The self-consistent potential also exhibits the same symmetry, with the spin-$\alpha$ potential at the top of the molecule being the same as the spin-$\beta$ at the bottom, and vice versa. This ensures that a superposition of this determinant with its $S_4$ image would have the proper spatial symmetry (although it would still not be a spin eigenfunction).

This calculation demonstrates that the restricted $D_{2d}$ solution is unstable, i.e., that even a small perturbation will not return to the restricted solution upon iteration but will proceed to a solution with a large spin asymmetry. This is probably not the most economical way to find such a solution, however, since we required ~100 iterations to obtain convergence. More experience is clearly needed to find good ways to speed up convergence; other work[31] suggests that it should be possible to construct initial guesses with larger spin asymmetries that are closer to the final results.

During the course of the SCF procedure, we found that round-off errors tended to destroy the potential symmetry mentioned above: the spin-$\alpha$ potential at the top began to drift away from the spin-$\beta$ potential at the bottom. To preserve the symmetry, we replaced the two potentials with their average every-second iteration. The more economical procedure (not employed here) would be to calculate and store only one of the two, accessing it when needed. In a similar fashion, only one member of each pair of degenerate $S_4$ image orbitals needs to be calculated, since the other can be constructed from it. With this procedure, a spatially unrestricted calculation is no more expensive than conventional spin-unrestricted calculations, except perhaps in being somewhat more difficult to converge.

(31) Noodleman, L.; Norman, J. G., Jr., personal communication.

Table III. Orbital Energies and Charges for $[Fe_4S_4^*(SH)_4]^{2-}$ ($T_d$ Symmetry)[a]

| | | charge distribution | | | |
|---|---|---|---|---|---|
| orbital | energy, eV | Fe | S | H | S* |
| $9t_2$ | −5.70 | 64.2 | 8.8 | 0.2 | 26.8 |
| $8t_2$ | −6.22 | 74.5 | 9.3 | 2.7 | 13.5 |
| $4t_1$ | −6.32 | 58.1 | 21.3 | | 20.6 |
| $4e^b$ | −6.60 | 41.2 | 51.7 | | 7.1 |
| $3t_1$ | −6.78 | 68.3 | 26.0 | | 5.7 |
| $7t_2$ | −7.33 | 48.0 | 49.4 | 0.6 | 2.0 |
| 3e | −7.85 | 78.9 | 20.3 | | 0.8 |
| $5a_1$ | −7.93 | 88.5 | 5.7 | 3.4 | 2.4 |
| $6t_2$ | −8.04 | 60.6 | 32.6 | 0.2 | 6.6 |
| $2t_1$ | −8.12 | 50.2 | 49.7 | | 0.1 |
| 2e | −8.45 | 71.2 | 26.2 | | 2.6 |
| $1t_1$ | −10.31 | 34.2 | 0.1 | | 65.7 |
| 1e | −10.34 | 24.8 | | | 75.2 |
| $5t_2$ | −10.86 | 37.4 | 0.3 | | 62.3 |
| $4t_2$ | −11.16 | 33.7 | 1.6 | 0.4 | 64.3 |
| $4a_1$ | −11.38 | 21.6 | 7.7 | 2.8 | 67.9 |
| $3t_2$ | −12.80 | 14.7 | 62.7 | 21.5 | 1.1 |
| $3a_1$ | −12.94 | 19.4 | 56.6 | 19.3 | 4.7 |
| $2a_1$ | −19.55 | 1.1 | 81.4 | 16.5 | 1.0 |
| $2t_2$ | −19.56 | 1.1 | 82.1 | 16.6 | 0.2 |
| $1t_2$ | −20.29 | 8.8 | 0.2 | | 91.0 |
| $1a_1$ | −20.62 | 11.1 | 0.9 | 0.1 | 87.9 |

[a] Charges, in percent of one electron, are calculated using the charge-partitioning scheme discussed in the Methods section. [b] Highest occupied orbital.

## Restricted MO Results

In this section we present our results for calculations assuming a molecular orbital model incorporating both spin and space restrictions, i.e., we require that the spin-$\alpha$ and spin-$\beta$ orbitals have the same spatial component and that all of the orbitals transform as irreducible representations of the $T_d$ or $D_{2d}$ point group of the nuclei. Although it is clear that such a model cannot provide a fully satisfying description of these clusters, it is of qualitative usefulness in understanding the nature of the chemical bonding and in assignments of excited states. Furthermore, previous theoretical discussions have assumed such a model, and useful comparisons between different computational approaches can be made.

A molecular orbital diagram for three computations on $[Fe_4S_4(SH)_4]^{2-}$ assuming $T_d$ symmetry is shown in Figure 2. The first two columns represent a "cube" geometry assumed in an earlier calculation[8] (geometry **1**) and compare touching and overlapping sphere results. These were discussed above, and suggest that the choice of sphere radii is not critical for these clusters. The final column uses overlapping spheres and a more "realistic" $T_d$ structure (geometry **2**). Although the overall molecular orbital pattern is similar, there are some important rearrangements that affect the conclusions one would draw from this picture. The most dramatic change comes in the 4e orbital, which is the lowest unoccupied orbital in the cube geometry and has 63% iron character (along with 25% on the organic sulfurs and 12% on the inorganic sulfurs). On going to the more realistic geometry, this orbital drops in energy relative to the others, becoming 41% Fe, 52% organic S, and 7% inorganic S. (Charge distributions for this realistic structure are given in Table III.)

This change has two important consequences. First, it predicts a much larger involvement of sulfur character in the top occupied orbitals, making qualitative pictures based on iron orbitals alone less reliable (see below). Second, it yields a top occupied orbital that is completely filled, in contrast to the cube geometry, in which the top occupied orbital (containing four electrons) is the triply degenerate $8t_2$ orbital.[8] While the cube geometry would be susceptible to a Jahn–Teller distortion, driving it to $D_{2d}$ symmetry,

Table IV. Orbital Energies and Charges for $[Fe_4{}^*S_4{}^*(SH)_4]^{2-}$ ($D_{2d}$ Symmetry)[a]

| orbital | energy, eV | charge distribution | | | |
|---|---|---|---|---|---|
| | | Fe | S | H | S* |
| $9b_2$ | −4.69 | 63.0 | 14.8 | 0.1 | 22.1 |
| 13e | −4.78 | 61.6 | 13.2 | | 25.2 |
| $8b_2$ | −5.11 | 73.6 | 5.6 | 0.5 | 20.3 |
| 12e | −5.14 | 72.7 | 11.6 | 0.2 | 15.5 |
| $4a_2$ | −5.56 | 65.2 | 10.8 | | 24.0 |
| 11e | −5.65 | 72.8 | 2.6 | 0.2 | 24.4 |
| $4b_1$[b] | −5.97 | 49.4 | 43.3 | | 7.3 |
| $3a_2$ | −5.98 | 73.6 | 24.2 | | 0.2 |
| 10e | −6.28 | 81.0 | 17.5 | 0.6 | 0.9 |
| $9a_1$ | −6.30 | 63.2 | 35.0 | 0.1 | 1.7 |
| $8a_1$ | −6.51 | 87.2 | 4.7 | 1.4 | 6.7 |
| 9e | −6.66 | 82.7 | 13.8 | 0.4 | 3.1 |
| $7b_2$ | −6.82 | 92.5 | 2.3 | 0.5 | 4.7 |
| $3b_1$ | −7.10 | 88.5 | 11.5 | | |
| $7a_1$ | −7.33 | 98.1 | 0.5 | 0.5 | 0.9 |
| 8e | −7.43 | 35.2 | 59.8 | | 5.0 |
| $2a_2$ | −7.51 | 38.4 | 61.6 | | |
| $2b_1$ | −7.78 | 55.2 | 42.8 | | 2.0 |
| $6b_2$ | −8.41 | 35.7 | 63.7 | 0.6 | |
| 7e | −8.47 | 37.1 | 60.9 | 0.5 | 1.5 |
| $6a_1$ | −8.59 | 46.0 | 45.4 | 0.4 | 8.2 |

[a] See footnotes to Table III. [b] Highest occupied orbital.

the more realistic $T_d$ geometry would be expected to have no static Jahn–Teller effect. Since the latter geometry is much closer to that seen in proteins and model compounds and has a calculated total energy 0.9 eV lower than that of the cube geometry, it would appear that arguments based on the Jahn–Teller theorem derive from a poor choice of geometry in the earlier calculation.

This point is of some interest in the interpretation of experimental magnetic susceptibility results.[32] These show that at low temperatures the clusters are diamagnetic and that excited paramagnetic states are thermally accessible. Yang et al.[8] considered this small energy difference between ground and excited states to be the result of a small splitting of the $8t_2$ orbital upon distortion from $T_d$ geometry. The present results do not allow for such a possibility. Similar conclusions have been reached by Geurts et al.[10] from extended Hückel and discrete variational X$\alpha$ calculations (discussed below). In fact, we show below that the MO model actually predicts a high-spin, paramagnetic ground state. We conclude that the explanation of the thermal paramagnetism cannot come from a restricted MO model but requires a more flexible wave function that can describe antiferromagnetic coupling among the iron atoms. This will be discussed in detail in the next section.

The descent from $T_d$ to $D_{2d}$ symmetry is illustrated in Figure 3, where the qualitative character of MO energy levels is indicated. A more detailed charge breakdown for the levels near the Fermi level is given in Table IV. The 4e level in $T_d$ symmetry splits into $9a_1$, which has 63% iron character, and $4b_1$, which has 49% iron character. There is a general increase in the iron character of levels near the Fermi level, but otherwise very little change from the $T_d$ results. One point in common that is of some interest is that the lowest unoccupied orbital ($4t_1$ in $T_d$ or 11e in $D_{2d}$) has about 20% inorganic sulfur character. This may be of some importance in understanding the properties of reduced clusters; this point will be considered in a future paper.

All of the results discussed up to now have been for a model $[Fe_4S_4(SH)_4]^{2-}$, with hydrogens attached to the organic sulfurs. We have also investigated the effects of replacing these with methyl groups, giving the model $[Fe_4S_4(SCH_3)_4]^{2-}$. In the earlier multiple-scattering calculations, a large effect had been seen upon replacing hydrogens with methyl groups (with an Fe–S–C angle of 180°): the amount of iron character in the top occupied orbitals decreased significantly, showing a much greater covalent mixing

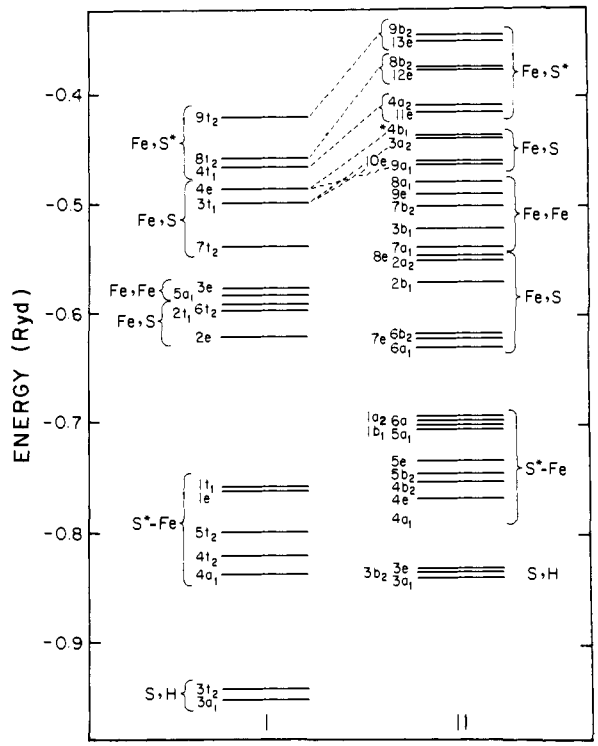


**Figure 3.** Molecular orbital energies for $[Fe_4S_4(SH)_4]^{2-}$: column I gives results for $T_d$ geometry, **2**, while column II gives results for the $D_{2d}$ geometry, **3**.

with the organic sulfurs.[8] On the other hand, extended Hückel calculations on the four-iron clusters[10] and X$\alpha$ calculations on analogous one-iron clusters (rubredoxin models)[6] showed only very small effects with this change.

Accordingly, we have compared the results of two spin-restricted MO calculations, one with hydrogens and one with methyls, using geometries **3** and **4** as defined in Table I. Only small differences are seen. Total atomic charges for the –H and $-CH_3$ calculations are 26.29 and 26.26 (Fe), 16.08 and 16.07 (S*), 16.25 and 16.18 (S). The average iron character in the top occupied orbitals *does* decrease, but only by 6%. This is smaller than the changes seen with different geometries (see below). Of course, the S–H band of orbitals disappears, being replaced by S–C and C–H orbitals, but these are fairly low in energy and do not affect the characters of orbitals near the Fermi level.

Two explanations may be proposed for the earlier results[8] that showed a large effect of methyl replacing hydrogen: first, that the sulfur atoms are more sensitive to such a change with artificial Fe–S–C bond angle of 180° than they are with bond angles near 103°; or second, that the small nonoverlapping spheres used by Yang et al. magnify the difference between the two groups. In both respects we feel the present results should be a more reliable guide to substituent effects.

**Comparisons to Qualitative MO Arguments.** Several qualitative molecular orbital arguments have been proposed to account for properties of clusters with four transition metals in a tetrahedral symmetry.[9,11,33] These generally assume that the strong metal–ligand interactions are found in a separate (lower) energy range and that the highest orbitals of the complex are primarily metal-like. Then it may be expected that the 20 metal 3d orbitals will cluster into three groups of symmetry orbitals: the first group, spanning $a_1 + e + t_2$ symmetries, have bonding metal–metal interactions and should lie lowest. A second group of six corresponding antibonding cluster orbitals, spanning $t_1 + t_2$, will be of higher energy. The remaining eight orbitals are formally nonbonding and span $e + t_1 + t_2$. These last orbitals will have

(32) Antanaitis, B. C.; Moss, J. H. *Biochim. Biophys. Acta* **1975**, *406*, 262. Cerdonio, M.; Wang, R.-H.; Rawlings, J.; Gray, H. B. *J. Am. Chem. Soc.* **1974**, *96*, 6534. See also, Ref. 27b for model complex results.

(33) Fourst, A. S.; Dahl, L. F. *J. Am. Chem. Soc.* **1970**, *92*, 7337. Gall, R. S.; Chu, C. T.; Dahl, L. F. *Ibid.* **1974**, *96*, 4019. Trinh-Toan; Teo, B. K.; Ferguson, J. A.; Meyer, T. J. *Ibid.* **1977**, *99*, 408.

energies primarily determined by interactions with the ligands and may be expected to lie either between the first and second sets, or higher than this, if the (antibonding) metal–ligand interactions are strong. For example, the configuration of $[Fe_4(\eta^5\text{-}C_5H_5)_4(\mu_3\text{-}S)_4]$ has been assigned $(a_1 + e + t_2)^{12}(t_1 + t_2)^8(e + t_1 + t_2)^0$, on the assumption that the relatively strong interaction between the cyclopentadienyl ligands and the metal would drive the third set of metal orbitals to higher energy.[33] On the other hand, for the core of interest here, $[Fe_4S_4(SR)_4]^{2-}$, the nonbonding orbitals have been assigned to a central position,[11] giving the configuration $(a_1 + e + t_2)^{12}(e + t_1 + t_2)^{10}(t_1 + t_2)^0$.

These predictions may be compared to the results of our $T_d$ calculations shown in Figure 2. We do find a reasonably large separation between the top orbitals, which are primarily iron-like, and the lower metal–ligand orbitals. This is especially true in the cube geometry (**1**), where the iron-like orbitals split neatly into the three groups described above; these are labeled 1–3 at the center of Figure 2. For the more realistic $T_d$ geometries, however, this model breaks down to a considerable degree, principally because the separation between metal and ligand orbitals is no longer so clear. For the cube geometry the average iron character in these top orbitals is 80%, but it drops to 65% in the more realistic geometry. The 4e orbital, in particular, changes from being 67% iron and 23% organic sulfur in the cube to being 41% iron and 52% sulfur in the latter geometry. These changes have the effect of scrambling the energy levels substantially from the simple picture, as can be seen in the right-hand side of Figure 2. Here, the 4e level, which was unoccupied in the cube geometry, is now the highest occupied level, while the $8t_2$ (nonbonding) level has moved up among the formally antibonding levels. Although these differences are not large ones, they are sufficient to make the qualitative models very tenuous for detailed predictions.

In the transition from the more realistic $T_d$ geometry to the $D_{2d}$ geometry, the fraction of iron character in the top orbitals increases again, to an average value of 75%. Nevertheless, the $D_{2d}$ results are closer to the realistic $T_d$ values than to the cube ones, as may be seen in Figure 3. The top occupied orbital is $4b_1$, which descends from the 4e orbital in tetrahedral symmetry and has 49% iron and 43% sulfur character. Thus, both the realistic $T_d$ and the $D_{2d}$ calculations show a HOMO with substantial sulfur character, and both predict that the $8t_2$ orbital (or its descendents $8b_2$ and 12e) will be unoccupied.

One important feature of the qualitative models that *is* in agreement with our calculations is that the highest occupied and lowest unoccupied orbitals are formally nonbonding; for these clusters this implies an antibonding interaction toward one neighboring iron and a bonding interaction toward the others. This can be seen clearly in Figure 4a, where countours of the highest occupied orbital, $4b_1$ in $D_{2d}$ symmetry, are shown. On the left the (weak) antibonding interaction between the two irons at the top of the molecule may be seen, while on the right a bonding interaction between a top iron and a bottom iron is visible. Similar behavior is evident in Figure 4b for the lowest unoccupied orbital, 11e in $D_{2d}$ symmetry. Here, however, there is a bonding interaction between the irons at the top and an antibonding interaction from top to bottom.

To summarize these results, it appears that the amount of orbital mixing in these clusters is large enough to invalidate (at least in detail) models based only on metal–metal interactions. Furthermore, the energy level diagrams are quite sensitive to geometry, so that symmetry considerations alone are inadequate. Nevertheless, the broad outline of the simple models seems to hold, if attention is restricted to the qualitative features of the top orbitals, which are primarily metal-based. As we discuss below, however, the character of the orbitals near the Fermi level changes considerably in an unrestricted calculation, so that even the present computations have only qualitative significance.

**Comparison to Previous Calculations.** We have already discussed the relationship of the present results to earlier scattered wave calculations of Yang et al.[8] More recently Geurts et al.[10] have reported Xα calculations on $[Fe_4S_4(SH)_4]^{2-}$ using a linear combination of atomic orbitals (LCAO) approach rather than the

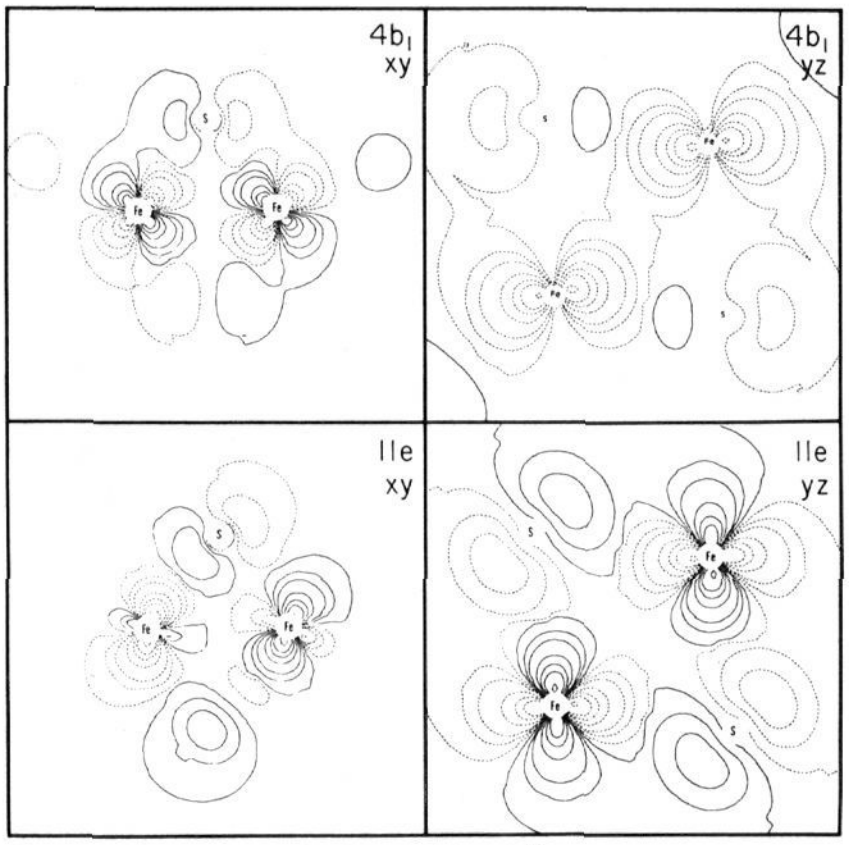


**Figure 4.** Contour maps for $[Fe_4S_4(SCH_3)_4]^{2-}$. (a, Top) Highest occupied orbital ($4b_1$). *xy* gives a plane passing through two irons and one sulfur at the top of the molecule. *yz* shows a plane parallel to the $S_4$ axis passing through irons at the top and bottom of the molecule. Projections of the sulfur atoms onto the plane of the figure are indicated. Contours are ±0.3, ±0.2, ±0.15, ±0.1, ±0.05, ±0.03, and ±0.01. Negative values are indicated by dashed lines. (b, Bottom) Lowest unoccupied orbital (11e).

multiple scattering approximations. In this method the matrix elements are all calculated numerically, and the α factor in the exchange potential is taken to be 0.7. The core orbitals are either frozen or are represented by a pseudopotential. The valence basis set is of double-ζ Slater-type orbitals. The geometry chosen by these workers is essentially identical with our geometry **2**.

The results of the two calculations are extremely close, as may be seen by comparing our Figure 3 with the "frozen core" results of Figure 2 in ref 10. If the LCAO–Xα results are shifted downward by 10 eV (they used no Watson sphere to stabilize the anion), the two calculations show energy levels and orbital compositions that are nearly identical. The largest orbital energy difference is ≲0.5 eV, and the average differences are much smaller. Two small differences may be of some importance. First, the width of the band of orbitals containing S* 3p character ($4a_1$ to $1t_1$ in Figure 3) is less in the multiple-scattering calculation than in the LCAO results. This may have some effect on the interpretation of the optical spectrum, as we discuss below. Second, three sets of neighboring levels are reversed in energy in the two calculations. These are $4t_1$ and $8t_2$, 4e and $3t_1$, and 3e and $7t_2$. In each case the splitting is small in both calculations, so that it is hardly surprising that such differences might be found. These changes do serve to change the symmetry designations of the HOMO and LUMO but do not alter any of the qualitative conclusions one would derive from the computations. It would be difficult in any event to decide which ordering was correct, since both computations have errors, muffin tin approximations in our case and basis set limitations and numerical inaccuracies in integral evaluations in the case of the LCAO results.

Geurts et al. compared their results to earlier multiple-scattering calculations of Yang et al.[8] and concluded that there were significant differences, both near the Fermi level and in terms of separations between clusters of Fe 3d, S 3p, and S* 3p like orbitals. The present results show that this is not a result of intrinsic differences in the two methods of calculation but arose principally from the differences in geometry of the two calculations being compared.

Two other types of molecular orbital calculation have also been reported for $[Fe_4S_4(SH)_4]^{2-}$. One used the LCAO–Xα method with a pseudopotential replacing the core electrons, while the other

used the extended Hückel scheme.[10] Both of these results are quite different from the two compared above. The pseudopotential levels near the Fermi level differ significantly from the ones shown here, and there appears to be no way to occupy the orbitals such that all of the occupied orbitals are below all the unoccupied ones. This complicates the search for the ground state and makes it impossible to classify the excited states in any reasonable manner. In general, the differences between the frozen core LCAO–X$\alpha$ and the pseudopotential LCAO–X$\alpha$ are much larger than are the differences between the frozen core LCAO–X$\alpha$ and the present multiple-scattering results.

Geurts et al. have also reported extended Hückel calculations for these complexes[10] that differ considerably from the X$\alpha$ results. In the extended Hückel calculation, there is little mixing between the iron orbitals and those of the organic sulfurs, and a large energy gap is found between the Fe d band and the S or S* 3p band. The predicted frequencies for the charge-transfer bands are much too high in the Hückel calculation, compared to what are believed to be the correct assignments (see below). Further comparisons of the Hückel and X$\alpha$ calculations may be found in ref 10.

Very recently, Thomson[9] discussed the ESR and magnetic susceptibility results of these clusters in terms of a simple MO model in which the iron–sulfur and iron–iron interactions are treated as adjustable parameters. He proposes the following d-level ordering: $a_1^2 < t_2^6 \sim t_2^6 < e^4 < e^4 < t_1^0$. This is not in accord with the order we find (see the right-hand column of Figure 2); where Thomson proposes that two orbitals of $t_2$ symmetry are occupied, we find one $t_1$ and one $t_2$ orbital. This model *does* agree with ours in having an e orbital as the highest occupied and a $t_1$ orbital as the lowest unoccupied. Thomson argues that this pattern rationalizes the g-tensor data for the 1- and 3-odd-electron species. Since the order of the lower-lying orbitals is irrelevant to his argument, a similar rationalization could be made on the basis of the results obtained here. Nevertheless, we continue to be dissatisfied with the MO model and will argue in favor of less restrictive wave functions in the next section.

Like Guerts et al.,[10] Thomson criticizes the orbital energy diagram of the earlier X$\alpha$ multiple-scattering calculations.[8] Since we have seen that these used an unrealistic cube geometry, such criticisms should be considered as directed against a particular calculation and not against the X$\alpha$ method itself.

In summary, we believe that the "frozen-core" LCAO–X$\alpha$ and the present multiple-scattering results offer the most accurate MO picture for the complexes. The overall agreement between LCAO–X$\alpha$ and multiple-scattering X$\alpha$ results suggests that muffin-tin errors are not of great importance here and give us confidence in the extension of multiple-scattering techniques to UHF wave functions, which have not been attempted previously.

**Optical Spectra.** The electronic spectra of both 4-Fe and 8-Fe proteins are characterized by two prominent bands at 380–400 and 290 nm.[34] Counterparts of these protein maxima are found at ca. 415 and 300 nm for the $[Fe_4S_4(SR)_4]^{2-}$ analogues.[35] When the proteins are placed in denaturing medium (80% $Me_2SO$ in $H_2O$), the lower energy absorption maxima moves to the interval 400–410 nm, indicating that at least some of the difference between the analogues and the proteins is due to the tertiary structure of the proteins.[36]

In addition to these intense bands, a variety of weaker absorptions are also seen. For the model compounds, one is in the 650–700-nm region, while an additional feature is seen near 350 nm.[35] The spectrum in the solid state shows bands between 500 and 600 nm that are not well-resolved in the solution spectrum and an additional band at about 800 nm that is not observed at all in solution.[35] Circular dichroism and magnetic circular dichroism studies of the proteins show that the region between 300 and 600 nm, although dominated by one intense band, contains three or more individual transitions.[37] Finally, the reduced form of the high-potential proteins shows a long-wavelength feature at 1040 nm that appears to have no counterpart in the analogues.[38]

In view of the relative lack of detail in the experimental spectra and of the large number of transitions that are possible in such a dense molecular orbital diagram, it is futile to attempt to make detailed assignments. Indeed, these clusters are sufficiently large that a solid-state-like "band" description becomes appropriate, in which broad features are assigned to transitions of a certain character (e.g., S → Fe charge transfer, iron d → d, etc.) rather than to individual molecular excited states.

Here we use our molecular orbital results for $[Fe_4S_4^*(SH)_4]^{2-}$ to provide such a description. The relevant energies are shown in Figure 3, and the orbital characters are given in Table III. Because of the extensive delocalization of these molecular orbitals, relaxation effects are expected to be small for the valence band transitions.[10,29] For this reason, we may avoid transition-state calculations (which incorporate orbital relaxation effects) and consider instead one-electron energy differences among the ground-state orbitals. Geurts et al. have shown that these two procedures differ by less than 3% for these clusters.[10]

Following this procedure, the strong transition in the 280–300-nm region may be assigned to a charge transfer transition from the inorganic sulfur (S*) 3p into the iron d orbitals. This involves promoting an electron from the bonding S*–Fe band (orbitals $4t_1$ to $9t_2$ in Figure 3). This yields a net charge transfer, since the lower orbitals are primarily localized on the S* centers while the upper orbitals have more charge density at Fe (see Table III). The longest wavelength transition of this type ($1t_1 \rightarrow 4t_1$) lies at 310 nm, while the center of the group should lie near $5t_2 \rightarrow 8t_2$, which is calculated at 270 nm. The right-hand side of Figure 3 shows that this prediction is affected very little by going to the $D_{2d}$ geometry, since both the S*–Fe and Fe–S* band rise by about 0.06 Ryd (0.8 eV).

The lower-energy strong transition near 380–400 nm is most likely also of charge-transfer origin, this time from the lower "Fe–S" band (orbitals $2e–6t_2$) into the same set of unoccupied orbitals ($4t_1–9t_2$). These transitions contain a strong component of metal d–d character, being primarily transitions from bonding Fe–S orbitals into antibonding Fe–S* orbitals (see Table III). In the tetrahedral geometry, these transitions are calculated to be at lower energy than the observed band: even the highest transition ($2e \rightarrow 9t_2$) is calculated to lie at 450 nm, to the red of the observed transition. However, in this case the change from $T_d$ to $D_{2d}$ geometry is larger than before (compare the left- and right-hand sides of Figure 3). In the $D_{2d}$ geometry, the bottom of the Fe–S band stays nearly constant, while the antibonding unoccupied levels ($11e–9b_2$) rise by about 0.8 eV. This raises the energy of this type of charge-transfer transition into the experimental range of 380–400 nm. This widening of the Fe–S band is probably a result of changing the Fe–S–H bond angle from 180° in the $T_d$ structure to 103° in the $D_{2d}$ geometry, a change that would allow a much more realistic representation of the organic sulfur lone pairs.

This assignment of the two strong bands as sulfur to metal charge transfer agrees with that postulated by most experimental workers[34,35] and is also in accord with the conclusions of the LCAO–X$\alpha$ calculations.[10] In the latter calculation, the energy gap between the 2e and $9t_2$ levels was about 0.5 eV higher than that obtained here for the $T_d$ geometry, so that it was not necessary to invoke a symmetry lowering to $D_{2d}$ in order to assign the 380–400-nm band as S→Fe charge transfer. Although it is impossible to assign a single cause to the difference between the two calculations, it appears to be connected to the appearance of a large gap of about 1.7 eV in the multiple-scattering results between the $1t_1$ and 2e orbitals (i.e., between the top of the S*–Fe band and the bottom of the Fe–S band; see Figure 3). In the LCAO–

(34) Hong, J. S.; Rabinowitz, J. C. *J. Biol. Chem.* **1970**, *245*, 4982.
(35) DePamphilis, B. D.; Averill, B. A.; Herskovitz, T.; Que, L., Jr.; Holm, R. W. *J. Am. Chem. Soc.* **1970**, *96*, 4159. Holm, R. H.; Averill, B. A.; Herskovitz, T.; Frankel, R. R.; Gray, H. B.; Sliman, O.; Grunthaner, F. J. *J. Am. Chem. Soc.* **1977**, *96*, 2644.
(36) Que, L., Jr.; Holm, R. H.; Mortenson, L. E. *J. Am. Chem. Soc.* **1975**, *97*, 463.
(37) Stephens, P. J.; Thomson, A. J.; Dunn, J. B. R.; Keiderling, T. A.; Rawlings, J.; Rao, K. K.; Hall, D. O. *Biochemistry* **1978**, *17*, 4770.
(38) Cerdonio, M.; Wang, R. H.; Rawlings, J.; Gray, H. B. *J. Am. Chem. Soc.* **1974**, *96*, 6534.

Xα calculation this gap is only about 1.2 eV wide, so that the 2e orbital is effectively lower in the LCAO results than in the multiple-scattering calculation. (In the multiple-scattering approximation this gap is considerably reduced upon going to $D_{2d}$ symmetry, so that it may be of little experimental significance. The LCAO–Xα calculations considered only $T_d$ geometries.)

The low intensity peak at about 690 nm seems most likely to arise from iron d–d transitions, from the $6t_2$ or $5a_1$ orbitals into $8t_2$ or $4t_1$. These transitions are calculated to lie between 680–730 nm. The longer wavelength transitions at 800 and 1040 nm are also likely to be of this type. Likely possibilities are $3t_1 \rightarrow 4t_1$, calculated to be at 810 nm, and $7t_2 \rightarrow 8t_2$, predicted to lie at 1120 nm. Identifying these transitions with the qualitative label "iron d–d" is of course a simplification, since there is a substantial amount of sulfur character in almost all of the orbitals (see Table III). These assignments of the low energy transitions are also in accord with the conclusions of Geurts et al.[10]

We have based these qualitative assignments on the spin-restricted MO results shown in Figures 2 and 3. In principle, we would like to provide a similar analysis based on the unrestricted wave functions to be discussed below, since we believe these to be more realistic functions. However, these broken symmetry solutions are mixed spin states whose energies are weighted averages of various pure spin multiplets. In order to assign opitcal spectra the energies of the pure spin states must be extracted; this is usually done by spin-projection techniques.[19] This procedure requires information about the overlaps among various orbitals and is rather complicated to apply in cases as complex as the present one. In the simplest approximation, we could ignore the changes introduced by spin projection and estimate excitation energies from the one-electron energies of the unrestricted wavefunction. This procedure yields assignments identical with those discussed above, and for this reason we shall not give the details of such a calculation here. A more complete analysis would also consider the possibility of localized transitions from the sulfur lone pairs.[39] Results of such calculations will be reported in a future publication.

### Unrestricted Results

We mentioned above that many of the experimental results on these iron–sulfur clusters are easier to understand on the basis of a valence bond picture like that shown in Figure 1 rather than in terms of conventional restricted MO theory. In its simplest form, this model consists of a two-configuration wave function, the one depicted in Figure 1 plus its $S_4$ image in which the top and bottom iron atoms have been interchanged. In this way the spin density vanishes at every point in space. (Such a two-configuration wave function is not a spin eigenfunction, but a singlet state could be projected from it, as we discuss below.) All four iron atoms are equivalent, but strong spin correlations exist: the spin-α electron tend to be localized at the top of the molecule when the spin-β electrons are at the bottom, and vice versa. It is this spin correlation that is not included in the restricted MO wave function.

This idealized picture still has fairly high symmetry: within each of the two configurations the orbital symmetry is $C_{2v}$, with the iron atoms equivalent in pairs; furthermore, the α and β orbitals are related by the $S_4$ symmetry operation, so that in the final wave function all four iron atoms are equivalent. Several pieces of experimental evidence support the notion that a descent to even lower symmetries is not necessary. The crystal structures of model complexes[27] closely approximate a $D_{2d}$ structure in which the local geometry about each iron atom is the same. This appears to rule out trapped valence structures in which there are distinct Fe(II) and Fe(III) sites. Moreover, Mössbauer spectra show only one iron signal,[5,12] which also argues against lower symmetry wavefunctions.

There are four main pieces of evidence against the restricted MO model that support the existence of strong spin correlations.

Table V, Charge and Spin Distributions[a] for $[Fe_4S_4^*(SCH_3)_4]^{2-}$

| | atom | | | | |
|---|---|---|---|---|---|
| | Fe | S* | S | C | H[b] |
| (A) Total Valence Charges, Spin-Restricted ($D_{2d}$) Calculation | | | | | |
| s | 0.47 | 1.84 | 1.76 | 1.14 | 1.09 |
| p | 0.53 | 4.23 | 4.41 | 2.59 | |
| d | 7.26 | | | 0 | |
| total[c] | 26.26 | 16.07 | 16.18 | 5.73 | 1.09 |
| (B) Total Valence Charges, Broken Symmetry ($C_{2v}$) Calculation | | | | | |
| s | 0.50 | 1.84 | 1.76 | 1.13 | 1.09 |
| p | 0.60 | 4.42 | 4.42 | 2.59 | |
| d | 6.95 | | | | |
| total[c] | 26.05 | 16.27 | 16.18 | 5.73 | 1.09 |
| (C) Spin Populations,[d] Broken Symmetry ($C_{2v}$) Calculation | | | | | |
| s | 0.027 | 0.002 | 0.004 | 0.000 | 0.010 |
| p | 0.118 | 0.055 | 0.383 | 0.016 | |
| d | 2.774 | | | | |
| total | 2.919 | 0.057 | 0.386 | 0.016 | 0.010 |

[a] Populations determined using the charge-partitioning scheme discussed in the Methods section. [b] Average values for the (inequivalent) hydrogens are given. [c] Includes core contributions. [d] Values are for the top of the molecule; spin populations at the bottom are the negatives of those shown.

First, in the odd-electron species formed by oxidation or reduction of the $Fe_4S_4^{2+}$ core, Mössbauer spectra reveal internal contact fields at the iron nuclei of opposite signs.[5,12] This is direct evidence of spin separation in the odd-electron complexes and implies that similar behavior may exist in the even-electron species as well. Second, magnetic susceptibility measurements point to the existence of low-lying paramagnetic excited states. As we discuss in more detail below, this would be expected in the valence bond picture: changes in the spin-correlation pattern (with relatively little change in the charge distribution) may occur with only small energy penalties. In the restricted MO model, it is difficult to rationalize the presence of thermally accessible paramagnetic states (see the previous section). Third, the paramagnetic NMR shifts are proportional to the magnetic susceptibility, as one would expect for antiferromagnetic coupling.[27c] Finally, the calculations here show that the restricted solution is very unstable, with the total energy decreasing by 2.5 eV in going from the restricted to the unrestricted wave function. While the results of approximate quantum mechanical calculations should not be given the same weight as careful experimental studies, this conclusion is in agreement with much experience in antiferromagnetic interactions in transition-metal complexes.[15] In particular, the existence of strong antiferromagnetic spin correlation in the 2Fe–2S clusters is well established;[40] since the geometry of the bridging sulfur ligands is nearly the same in the 2Fe and 4Fe clusters, similar antiferromagnetic interactions may be expected in each.

**Broken Symmetry Orbitals.** Our unrestricted calculations go beyond the idealized model of Figure 1 by allowing the amount and location of the spin separation to be determined by the self-consistent procedure. Thus we may expect that the spin on each iron will be less than the idealized value of 4.5, and that some of the spin will be found on the sulfur atoms. Charge and spin populations are given in Table V. These show that only a small amount of charge redistribution takes place on going from the $D_{2d}$ to $C_{2v}$ solution: each iron atom gives about 0.2 electron to the S* 3p orbitals. Most of the spin population is in the iron d orbitals, but the spin separation is only 2.77/4.5, 62% complete. (An alternative measure of the extent of spin separation may be obtained by considering excess spin on all of the atoms listed in Table V. This yields 3.39/4.5, 75%.) There is some unpaired electron character in the S 3p orbitals, but it is only 14% as great as that in the Fe d orbitals, justifying to a large extent the simple picture given in Figure 1.

Orbital energies from the broken symmetry calculation are shown in Figure 5. We can distinguish orbitals that are located

(39) See, for example: Nitsche, L. E.; Davidson, E. *Chem. Phys. Lett.* **1978**, *58*, 171. Martin, R. L. *J. Chem. Phys.* **1981**, *74*, 1852.

(40) Sands, R. H.; Dunham, W. R. *Q. Rev. Biophys.* **1974**, *7*, 443.

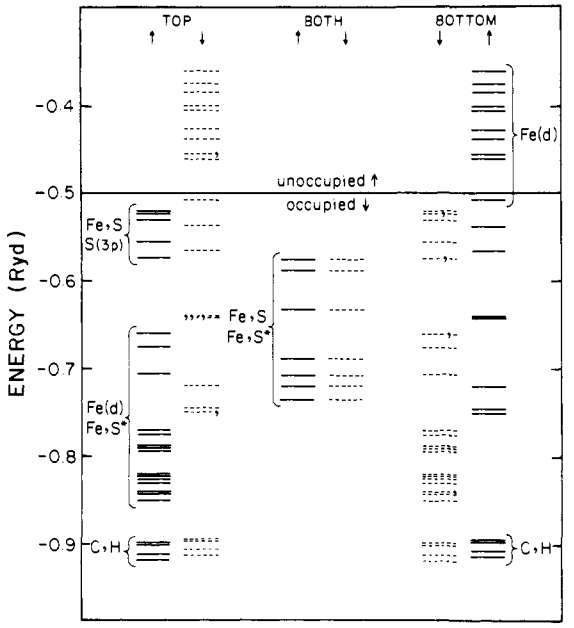


**Figure 5.** Orbital energies for $[Fe_4S_4(SCH_3)_4]^{2-}$ in the broken symmetry calculation. Spin-$\alpha$ orbitals have a solid line, spin-$\beta$ a dashed line. The division into top, bottom, and both is discussed in the text.

predominately at the top or bottom of the molecule from orbitals that have a more even distribution of charge at both top and bottom. (It should be clear that no rigorous dividing line can be drawn. We have labeled "top" those orbitals whose top/bottom charge asymmetry is 75/25 or greater.) On the left are shown the orbitals located predominantly at the top of the molecule; those at the right are located at the bottom; orbitals with an even top/bottom distribution are shown in the center. Spin-$\alpha$ orbitals are given as solid lines, spin-$\beta$ as dashed lines. The symmetry of the molecule is evident: for every $\alpha$ orbital at the left, there is a degenerate $\beta$ orbital at the right. These two orbitals are $S_4$ images, as discussed under Method.

As expected, the exchange splittings between $\alpha$ and $\beta$ iron d orbitals are large. At the top of the molecule, the spin-$\alpha$ d orbitals are centered at −0.75 Ryd, whereas the spin-$\beta$ orbitals are centered at −0.43 Ryd and are unoccupied except for the lowest orbital of this group. The idealized description ascribes ten spin-$\alpha$ electrons and one spin-$\beta$ electron to the two irons at the top of the molecule. These are completely delocalized, i.e., each iron atom has an effective formal charge of 2.5+. The bottom of the molecule is the analogue of the top, with $\beta$ replacing $\alpha$. The total $M_s = 0$ wave function consists of the configuration illustrated in Figure 5 plus its $S_4$ image.

Figure 5 also shows that the exchange forces also have a marked effect on the character of the molecular orbital diagram. The spin-$\alpha$ iron d orbitals are driven down below the Fe–S and S (lone-pair) type orbitals, while the spin-$\beta$ iron d band is higher in energy and is mostly unoccupied. Thus, the highest occupied molecular orbitals no longer have the large amount of iron character found above for the MO wave functions. Populations for the broken symmetry orbitals are given in Table VI. These confirm the pattern seen earlier[6,7] in spin-unrestricted calculations on 1-Fe and 2-Fe iron–sulfur clusters: the lowest unoccupied orbitals are primarily iron d orbitals, while the highest occupied are predominantly sulfur in character. There is one exception to this generalization: the highest occupied orbital for the 4-Fe cluster (20a, in Table VI) is predominantly iron 3d in character, so that the sulfur character begins only with the next lower occupied orbital ($13b_2$). This is easily understood from electron counting considerations. The oxidized forms of the 1-Fe and 2-Fe clusters are all Fe(III) in a formal sense, whereas the oxidized form of ferredoxins corresponds formally to 2-Fe(II) + 2-Fe(III). Hence a pair of minority-spin Fe d orbitals must be occupied in the 4-Fe clusters, whereas all minority spin d orbitals are unoccupied in the 1-Fe and 2-Fe clusters.

Table VI, Orbital Energies and Charges for $[Fe_4S_4{}^*(SCH_3)_4]^{2-}$ ($C_{2v}$ Symmetry)[a]

| | | charge distribution[c] | | | | | |
|---|---|---|---|---|---|---|---|
| | | Fe | | S | | S* | |
| orbital[b] | energy, eV | top | bottom | top | bottom | top | bottom |
| | | | (i) Bottom[d] | | | | |
| $14b_2$ | −6.17 | 4.2 | 81.2 | 0.8 | 1.2 | 10.6 | 1.0 |
| $9a_2$ | −6.24 | 3.4 | 71.6 | 0.4 | 12.6 | 9.4 | 1.8 |
| $20a_1$[e] | −6.89 | 1.8 | 86.8 | 1.8 | 3.4 | 0.6 | 4.0 |
| $13b_1$ | −7.31 | 17.2 | 3.4 | 3.4 | 51.6 | 3.6 | 16.0 |
| $7a_2$ | −7.68 | 0.4 | 33.4 | 0.0 | 59.4 | 0.4 | 0.0 |
| | | | (ii) Top[d] | | | | |
| $13b_2$ | −7.07 | 20.8 | 10.2 | 48.8 | 1.2 | 14.6 | 3.6 |
| $14b_1$ | −7.08 | 31.6 | 15.2 | 26.4 | 1.4 | 19.6 | 4.0 |
| $8a_2$ | −7.20 | 9.6 | 2.2 | 77.0 | 0.0 | 4.6 | 0.2 |
| $19a_1$ | −7.56 | 28.4 | 13.2 | 45.8 | 5.0 | 2.0 | 1.2 |
| $12b_2$ | −7.81 | 23.2 | 6.6 | 34.0 | 4.0 | 26.4 | 5.0 |
| | | | (iii) Both[d] | | | | |
| $12b_1$ | −7.83 | 24.2 | 22.2 | 8.2 | 19.8 | 7.4 | 13.4 |
| $18a_1$ | −8.00 | 43.4 | 13.8 | 3.2 | 1.2 | 12.4 | 23.6 |
| $6a_2$ | −8.60 | 31.0 | 21.2 | 5.8 | 0.2 | 11.6 | 28.6 |

[a] See footnote Table III. [b] All the orbitals shown are spin $\alpha$. Spin-$\beta$ populations may be obtained by symmetry. [c] Top and bottom refer to top and bottom of the molecule as in Figure 1. [d] Bottom, Top, and Both refer to the columns of Figure 5. Under Bottom are listed the three highest occupied molecular orbitals and the first two unoccupied orbitals. Under Top and Both the highest few occupied orbitals are shown. [e] Highest occupied orbital.

For the 1-Fe clusters, the general picture outlined in the previous paragraph has been supported by experiment[41] and by the results of GVB–CT calculations.[42] The analogies that may be drawn between the various clusters lead us to believe that this picture is valid here as well. A detailed comparison of the X$\alpha$ multiple-scattering results for these various iron–sulfur clusters is in preparation.

**Low-Lying Excited States.** We discussed above the magnetic susceptibility results on 4-Fe clusters, demonstrating the existence of paramagnetic excited states with substantial population at room temperature. It is customary to analyze these in terms of a spin Hamiltonian:

$$\mathcal{H} = -2J\mathbf{S}_1\cdot\mathbf{S}_2 \qquad (1)$$

Here $\mathbf{S}_1$ and $\mathbf{S}_2$ are the spins of weakly coupled monomers; in our case these would be the 2-Fe clusters at the top and bottom of the molecule. When $J < 0$, this describes antiferromagnetic coupling, with a ground-state singlet and a triplet excited state of energy $2J$ above the ground state. In the present case we may expect states of yet higher energies with larger values of $S$, up to a maximum of $S = 9$. This would correspond to the four iron atoms in the cluster having parallel spins, i.e., all the arrows would point up in Figure 1. Although it is unlikely that all of these levels could be fit exactly to the simple Heisenberg Hamiltonian, eq 1, there are reasons to believe that it should be approximately valid when the overlaps of the monomer orbitals (the iron 3d orbitals) are small, as they are here.[15,19]

It is only recently that concerted attempts have been made to calculate antiferromagnetic coupling constants for systems containing two or more transition-metal atoms. Several approaches have been tried, some using molecular orbital[43] or configuration interaction[44] theories, while others utilize ideas from effective exchange potential theories.[45] Noodleman[19] has considered the problem in terms of the energy difference between the singlet ground state and the state of highest multiplicity allowed in a

(41) Hoggins, J. T.; Steinfink, H. *Inorg. Chem.* **1976**, *15*, 1682.
(42) Bair, R. A.; Goodard, W. A., III *J. Am. Chem. Soc.* **1978**, *100*, 5669.
(43) Hay, P. J.; Thibeault, J. C.; Hoffmann, R. *J. Am. Chem. Soc.* **1975**, *97*, 4884.
(44) DeLoth, P.; Cassoux, P.; Daudey, J. P.; Malrieu, J. P. *J. Am. Chem. Soc.* **1981**, *103*, 4007.
(45) Ginsberg, A. P. *J. Am. Chem. Soc.* **1980**, *102*, 111.

formal sense (in this case the $S = 9$ state formed from coupling two $S = {}^9/_2$ subunits). According to eq 1 this difference is

$$E(S_{max}) - E(S = 0) = -S_{max}(S_{max} + 1)J = -90J \quad (2)$$

Noodleman argues that in the X$\alpha$ theory one can gain an estimate of the energy of the high-spin state by performing a spin-unrestricted calculation with $M_x = S_{max}$. Although this would not be a pure spin state, all of the states with $S > 9$ should be much higher in energy and thus should contribute little to the contamination of the unrestricted wavefunction. It is more difficult to obtain the energy of the singlet ground state, since the broken symmetry state with $M_x = 0$ is expected to have a large amount of spin contamination. Noodleman has shown, however, that a spin-projection technique may be used to estimate the energy of the singlet state from the calculated energy of the broken symmetry state.[19] When fit to a Heisenberg Hamiltonian, this procedure yields the following relation:

$$E(S_{max}) - E(\text{broken symmetry}) = -S_{max}{}^2J = -81J \quad (3)$$

The left-hand side of this relation can be determined from total-energy calculations of two multiple-scattering configurations. Because of the large value of $S_{max}$ in the present case, it makes little difference whether we adopt Noodleman's approach, eq 3, or take the simpler approximation of using eq 2 and assuming that $E(S = 0) \approx E(\text{broken symmetry})$.

To implement this scheme we hav performed a spin-unrestricted calculation on $[Fe_4S_4(SCH_3)_4]^{2-}$ with $M_s = 9$. Since all the iron spins are now parallel, the orbitals again have $D_{2d}$ symmetry. The occupation scheme may be most easily understood by reference to the right-hand column of Figure 3. (This figure is drawn with hydrogens rather than methyl groups on the organic sulfurs, but the orbital energy diagram for the methyl calculation is completely parallel to this one near the Fermi level.) In the MO calculation the top nine orbitals are unoccupied ($11e$–$9b_2$; we count the degenerate "e" orbitals twice). The next lower nine orbitals ($7b_2$–$4b_1$) are the highest occupied ones. The occupation scheme for the $M_s = 9$ calculation was obtained by removing a $\beta$ electron from the last nine occupied orbitals ($7b_2$–$4b_1$) and adding an $\alpha$ electron to the lowest nine unoccupied orbitals ($11e$–$9b_2$). Upon iteration, the exchange forces move the $\alpha$ orbitals down and the $\beta$ orbitals up. At the self-consistent solution, all the occupied orbitals are below all the unoccupied ones; for example, the (unoccupied) $7b_2\beta$ orbital is higher in energy than the (occupied) $9a_2\alpha$. The resultant charge distributions are fairly similar to those of the broken symmetry calculation, except that there is now ferromagnetic rather than antiferromagnetic coupling between the top and bottom of the molecule. The spin population on each iron atom rises from 2.92 in the broken symmetry wave function to 3.29 in the $M_s = 9$ wave function; the spin population on sulfur also rises, from 0.38 to 0.49. These are still considerably lower than the simple VB picture that puts a spin of 4.5 on each iron atom.

The total statistical energy of this $M_s = 9$ configuration is 15 300 $cm^{-1}$ higher than that of the broken symmetry state. Equation 3 thus gives $J \simeq -188$ $cm^{-1}$. If we adopt the alternative assumption of using eq 2 and ignoring spin contamination, we obtain $J = -170$ $cm^{-1}$. Both of these values are in fair agreement with the $J = -232$ $cm^{-1}$ obtained experimentally[27b] for the model complexes $[Fe_4S_4(SCH_2Ph)_4]^{2-}$ and $[Fe_4S_4(SPh)_4]^{2-}$. The protein data are less precise: for the reduced high-potential protein, magnetic susceptability measurements[32] indicate little population of paramagnetic excited states such that $|J| > 200$ $cm^{-1}$. These low-lying excited states should contribute strongly to the observed properties of the clusters: for $J = -188$ $cm^{-1}$, 18% of the clusters would be in the triplet state at room temperature.

Norman et al.[7] have used this same computational method to calculate the Heisenberg coupling constant for the oxidized state of 2-Fe clusters. Their results give $J = -265$ $cm^{-1}$, compared to experimental values ranging from $-149$ to $-183$ $cm^{-1}$ for proteins and model complexes. It is clear that the precision of the calculations is not as great as one would like, but the results *are* qualitatively consistent with the experimental magnetic susceptibilities. This is in marked contrast with the MO results, which predict no low-lying paramagnetic excited states, as we discussed above. Further studies are in progress to help determine the quantitative reliability of the present approach to the calculation of antiferromagnetic constants.

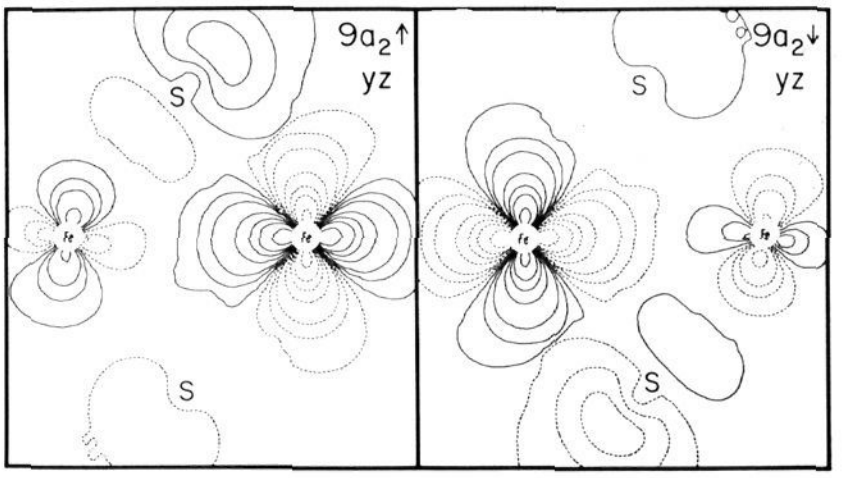


**Figure 6.** Contour maps for the lowest unoccupied orbital of the broken symmetry calculation. Plane shown is parallel to the $S_4$ axis passing through a top iron (at the left) and a bottom iron at the right. Contour values are the same as in Figure 4. Projections of the S atoms onto the plane of the figure are indicated.

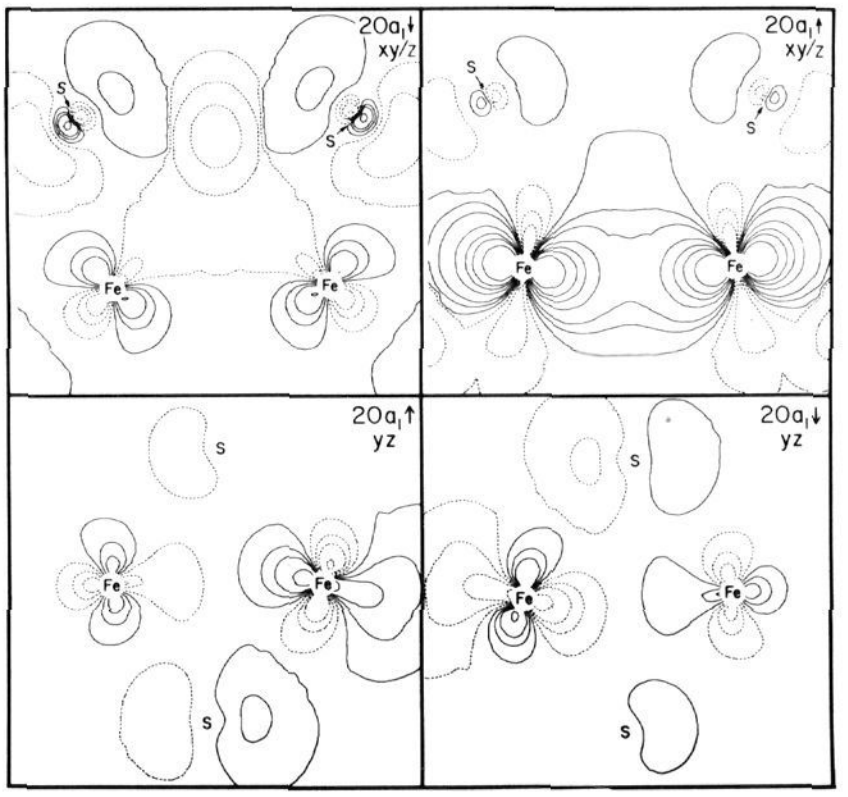


**Figure 7.** Contour maps for the highest occupied orbital of the broken symmetry calculation. (Top) Plane passing diagonally through the cube, containing the $S_4$ axis, two top sulfur atoms, and two bottom iron atoms. (Bottom) Same view as in Figure 6. Contour values are the same as in Figure 4.

We note, as an aside, that the total statistical energy of our $M_s = 9$ state is 0.6 eV lower than that of the $M_s = 0$ restricted molecular orbital wave function reported in the previous section. This implies that our MO model actually predicts the ground state to be a high-spin state, rather than a closed-shell singlet state. This bias of Hartree–Fock (or Hartree–Fock Slater) calculations toward high-spin states has been noted before.[46] It is only by considering broken symmetry states that we obtain an $M_s \simeq 0$ wave function with an energy below that of the paramagnetic states. Since it seems clear that the true ground state of this complex is diamagnetic, this is further evidence of the inadequacy of restricted MO theories for such weakly coupled clusters.

**Countour Maps.** Figures 6 and 7 show contour maps of orbitals from the broken symmetry calculation that illustrate some of the characteristic features of this wave function. Figure 6 shows the lowest unoccupied orbital ($9a_2$), in a plane parallel to the $S_4$ axis and passing through two irons, one at the top and the other at

(46) See, for example: Goodard, W. A., III; Olafson, B. D. *Proc. Natl. Acad. Sci. U.S.A.* **1975**, *72*, 2335. Goodard, W. A., III; Dunning, T. H., Jr.; Hunt, W. J.; Hay, P. J. *Acc. Chem. Res.* **1973**, *6*, 368.

the bottom of the molecule. This illustrates the spin separation one would expect from Figure 5: the spin-$\alpha$ orbital is mostly (86%) at the bottom of the molecule, while the spin-$\beta$ orbital is its $S_4$ image, being mostly at the top. There is a weak antibonding interaction between the two irons, and a stronger antibonding interaction with a bridging S* 3p is visible (the other S* atom is not in the plane of the figure). This is characteristic of a classical superexchange mechanism whereby bridging ligands lead to antiferromagnetic coupling of two metal ions.[47]

The bottom of Figure 7 shows a similar picture for the highest occupied orbital ($20a_1$). In this case the spin separation is even larger (94%), but the qualitative features are the same as for the $9a_2$ orbital. The top of the figure shows this orbital in a plane passing through two irons at the bottom and two sulfurs at the top of the molecule (a cut diagonally through the cube, passing through the $S_4$ axis). There is a weak bonding interaction between these two iron atoms, along with antibonding Fe–S* interactions.

Although we have not performed explicit calculations on the 1- or 3-Fe clusters, we would expect the odd electron in such complexes to be found in orbitals very much like those pictured in Figures 6 and 7. (Such an expectation was found to be correct in explicit calculations on reduced 2-Fe iron–sulfur clusters.[7]) We plan to report detailed results for the odd-electron clusters in a future publication. We do note that the S* antibonding interactions seen in Figures 4 and 7 are qualitatively consistent with the observed geometrical changes upon reduction of the model complexes: the principal effect of adding an electron to the 2–Fe clusters is to expand the S* shell, producing an elongated $D_{2d}$ structure.[27b] Little change is seen in the iron tetrahedron, consistent with the nonbonding character of the iron–iron interactions in these top orbitals. Furthermore, the inequivalence of the iron atoms in the oxidized and reduced species, which one would predict from Figures 6 and 7, is reflected in the inequivalent signals seen in the Mössbauer spectra.[5] None of the molecular orbital models that have been proposed[8-11] can easily account for such behavior, since they all force the irons to be completely equivalent.

## Conclusions

We have presented here X$\alpha$ multiple-scattering calculations on models for the active sites in oxidized 4-Fe ferrodoxins and reduced high-potential iron–sulfur proteins. These show that neither the simple MO nor VB model is completely adequate but that broken symmetry wave functions can be calculated with standard techniques and that these give a good qualitative account of the observed spectroscopic and magnetic properties of the complexes. We hope that this will be the first step in the development of new ways of thinking about the electronic structures of these clusters.

The active-site model considered here, with 270 electrons, is at the boarderline between molecular and solid-state problems. The energy level density is so large that for most purposes a band-theory description becomes appropriate, and we have relied heavily on such ideas for our interpretations. Although qualitative MO schemes reproduce many of the features we calculate, they appear to be unreliable for detailed arguments. It also appears that Jahn–Teller distortions are not responsible for the descent from $T_d$ symmetry and that they cannot be used to rationalize the observed magnetic susceptibilities. Our optical spectral assignments are in broad agreement with those suggested earlier, whereas the interpretation of the magnetic susceptibility results requires a wave function more complex than those considered previously.

The more complex wave function we have chosen, a broken symmetry UHF function, is clearly not the best possible one. Better functions would be spin eigenfunctions and would contain an explicit treatment of electron correlation. Unfortunately, it may be some time before such calculations are practical. Our present compromise has the advantage of being easy to visualize and of interpolating directly between the MO and VB limits. In this model the spin separation is 65–75% as large as in the idealized VB model, indicative of a truly intermediate structure.

Passing beyond the topics discussed here, we hope that these wave functions can form the foundation for the study of several other interesting properties:

**(a) Comparison of the Bonding Patterns in the 1-Fe, 2-Fe, and 4-Fe Clusters.** We now have available wave functions for all of these species at a common level of approximation. Work is in progress to prepare a detailed list of similarities and differences. One clear distinction exists in the odd-electron species: the 2-Fe clusters form trapped valence states with 1 Fe(II) and 1 Fe(III) center,[37] while the 4-Fe clusters appear to remain delocalized.

**(b) Variability of the Oxidation–Reduction Potentials in Different Proteins.** Although it does not appear feasible to attempt absolute calculations of such potentials, environmental effects such as local charge distributions or weak hydrogen bonds to the sulfurs can be included. Work is already in progress along these lines for the 2-Fe clusters (J. G. Norman, Jr., personal communication).

**(c) Study of Iron–Sulfur Clusters Outside the Electron-Transport Chain, Such As in Nitrogenase or Hydrogenase.** We hope that the orbital energy diagrams and contour maps presented here will make it possible to construct working interpretations of the Mössbauer, NMR, or chemical properties of similar clusters, even though they may not be identical with the symmetric, even-electron system considered here.

Our purpose in sketching these possible extensions (and there are others) is not to present a research proposal but to indicate our belief that computational quantum chemistry has entered an era in which such questions can fruitfully be attacked. Just a few years ago, even an approximate calculation of antiferromagnetic coupling constants for a four-iron system would not have been possible. Further advances and better quality wave functions will mark the future, but the molecular orbital based wave functions presented here should continue to provide useful insight into the nature of these important systems.

**Acknowledgment.** This work was supported by a grant from the National Institutes of Health, GM-26712. We thank Joe Norman and Keith Johnson for many helpful discussions and for providing us with the detailed results of their calculations. Louis Noddleman and P. Barry Ryan were very generous with advice on the theory and practice of performing broken symmetry calculations. We also thank Steve Sontum for assistance with some of the calculations.

**Registry No.** $[Fe_4S_4(SH)_4]^{2-}$, 73729-65-4; $[Fe_4S_4(SCH_3)_4]^{2-}$, 52261-30-0.

(47) Ballhausen, C. J. "Molecular Electronic Structures of Transition-Metal Complexes"; McGraw-Hill: New York, 1979; Section 3-6.